Large–Eddy Simulation of the Flow around the Free End of a Circular Cylinder

J. Fröhlich[1], W. Rodi[1], A. Dewan[2], and J.P. Fontes[3]

[1] Institut für Hydromechanik, Universität Karlsruhe, Kaiserstrasse 12, 76128 Karlsruhe, Germany, froehlich@ifh.uni-karlsruhe.de
[2] Indian Institute of Technology Guwahati, Guwahati-781039, India
[3] Électricité de France, 6 quai Watier, 78401 Chatou, France

Summary

The paper presents large–eddy simulations of the flow around a cylinder of finite height mounted on a flat plate. The Reynolds number is 43000 and the height–to–diameter ratio is 2.5. The computations were performed with two different Finite Volume codes and grids of different resolution. An analysis of the average and of the instantaneous flow is provided. Furthermore, the results are compared to a companion experiment.

1 Introduction

The computation of the turbulent flow around bluff bodies poses severe challenges due to the presence of massive separation with dominating anisotropic large–scale vortex systems. Under these circumstances large–eddy simulation (LES) is an approach capable of producing improved results compared to Reynolds–averaged methods due to the reduced amount of modelling which is traded against computational resolution and hence cpu time.

The present paper is the third in a series of papers concerned with the flow around circular cylinders. In the first [1] and part of the second [2], the flow around a long cylinder in uniform cross flow was studied. The main subject of [2] then was LES for a configuration in shear flow. In the following we report on investigations of the flow around a cylinder of finite height. The configuration corresponds to an experiment conducted by Kappler and Rodi [3], [4]. Such configurations have previously been simulated with steady RANS methods, e.g. [5]. Here, it is the first time that LES is applied to this flow.

2 Code development

The LES code LESOCC (**L**arge **E**ddy **S**imulation **O**n **C**urvilinear **C**oordinates) has been continuously developed at the Institute for Hydromechanics during the last years. While the computations in [1] were performed with the original sequential code developed in [6], the subsequent computations in [2] were performed with the

parallelized version, developed in [7]. The latter is based on the decomposition of a global, structured grid into an arrangement of sub–domains. In order to enhance the code's versatility and to improve its maintainance, the entire code, formerly in Fortran 77, was completely re–written in Fortran 90. It now makes use of essential features of the language such as dynamic allocation of memory, etc. The domain decomposition technique was generalized such that the structured curvilinear blocks can now be arranged in an arbitrary manner as long as neighbouring cells match. Very complex geometries can hence be handled, alleviated through an interface to the grid–generation software ICEM. For the configuration studied in the present paper this geometric flexibility was an important prerequisite.

The discretization in space employs a second order central Finite Volume scheme for all terms with collocated arrangement of variables. The momentum interpolation technique is used to avoid velocity–pressure decoupling, and a three–step Runge Kutta scheme is used for discretization in time.

3 Properties of the flow considered

The flow around a circular cylinder of finite height mounted on a flat plate is governed by several parameters: the Reynolds number Re (based on the diameter D and the free–stream velocity U_∞), the height–to–diameter ratio H/D, the free–stream turbulence level Tu, and the relative thickness of the flat–plate boundary layer δ/H. Here, we consider sub–critical flow at $Re = 43000$ with low turbulence level. For a long cylinder in uniform flow these conditions correspond to the "upper Transition in Shear Layer" regime ($Re = 2 \cdot 10^4 \ldots 2 \cdot 10^5$) [8]. It is characterized by a laminar boundary layer along the cylinder wall, laminar separation, and transition to turbulence in the shear layer shortly after separation through a Kelvin–Helmholtz instability and further spanwise instabilities. The structure and the average properties of the flow do not change much with the Reynolds number in this regime. It should be noted that this Reynolds–number range is highly relevant for industrial applications [8].

In contrast to the long cylinder case, the finite hight case introduces a very complex three–dimensional instantaneous and average flow. This is due to the two different types of end effects illustrated in Fig. 1. First, the flow over the free end intrudes into the recirculation region behind the cylinder and modifies its structure substantially. Near the tip, the vortex shedding is inhibited and two counter–rotating trailing vortices form [9]. The flow over the tip creates a strong downward motion in the rear which reduces the total drag compared to the long cylinder case substantially [10]. Second, any boundary layer developing along the ground plate creates a horse–shoe vortex around the base of the cylinder. If the cylinder is long enough a structure similar to the one of an infinitely long cylinder can develop in the middle section, between the tip region and the base region and regular vortex shedding of von Karman vortices is observed here. Kawamura et al. [9] determined a critical value of $H/D \approx 6$. Kappler [4] found a continuous transition in the vortex structure for the range $H/D = 2 \ldots 5$ characterized by an intermittent vortex shedding where the

percentage of regular antisymmetric vortices at half–height was still below 100% for $H/D = 5$.

Last but not least the parameter δ/H is of importance. In [9], D was fixed and H modified at constant δ, revealing that the tip vortices are reduced in magnitude and amount of downwash when H/D decreases. Smoke–wire photographs show that for $H/D = 8, \delta/H = 1/8$ the flow reattaches around the center of the cylinder roof whereas for $H/D = 4, \delta/H = 1/4$ no reattachment occurs. For $H/D = 1, \delta/H = 1$ reattachment again takes place. In [4] $\delta/H = 0.1$, and when D was altered the flow at the tip was independent of the resulting H/D and Re. We hence concentrate on the flow around the tip and neglect the influence of the ground–plate boundary layer.

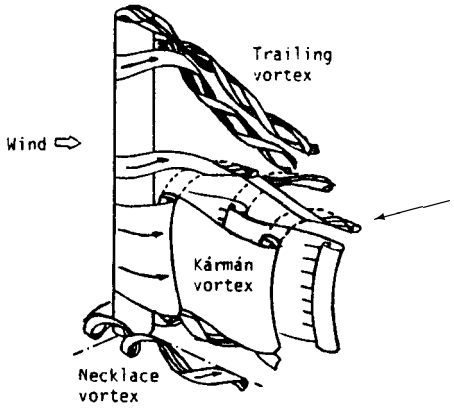

Figure 1 Sketch of the flow field around a cylinder of finite height longer than the critical length for vortex shedding, from [9]. The arrow points to the upper end of the von Karman vortices discussed in Section 5.1.

4 Computational setup

The geometric configuration studied here approximates a case investigated experimentally in [3], [4] with the following parameters: $Re = 43000$, $H/D = 2.5$, $\delta/H = 0.1$, $Tu = 2\%$. With the axis of the cylinder at $(x = 0, y = 0 \ldots 2.5, z = 0)$ and x the streamwise coordinate the size of the computational domain is $x = -7.5$ to $+12.5$, $y = 0$ to $+5$, $z = -3.5$ to $+3.5$. Throughout, the cylinder diameter and the free–stream velocity are used as length and velocity scales, respectively. The extent in y and z is equal to the size of the experimental testsection and introduces a blockage of 7.3%.

It should be noted that the present Reynolds number is fairly high compared to other LES of the subcritical flow around circular cylinders. An important issue is the resolution of the separating shear layer and its transition to turbulence. In an LES this can often only be accomplished marginally. On the other hand these regions are important for the downstream evolution of the flow.

Two computations were performed with two different meshes, a coarser one (LES1) with 1.0 Mio. and a finer one (LES2) with 6.4 Mio. interiour cells. Fig.2 gives an impression of the type of block structure and grid employed for LES1. The grid of LES2 was similar but refined close to the cylinder in x and z as well as in y (70 cells along the shaft, for example). The outflow boundary condition of the simulation is a convective one. The inflow condition is steady laminar flow, $Tu = 0$, which has been successfully used in previous LES for a long cylinder. In order to reduce the computational demands the bottom wall was assumed to be frictionless, thus avoiding the need to resolve the boundary layer there. This is justified to some extent by the small value of $\delta/H = 0.1$ in the corresponding experiment. Although, as a consequence, no horse–shoe vortex forms around the base of the cylinder, the flow around the tip should remain mostly unaltered. On the other hand, the results show that the flow in the wake becomes somewhat similar to the one with $H/D = 5$ and two free ends. The effective shaft region, less influenced by the end effects, is longer than in the case with bottom friction. For this reason we observe von Karman vortices as displayed below.

The subgrid–scale stresses were modelled with the Smagorinsky model using $C_s = 0.1$. In a separate computation the dynamic model was applied with relaxation in time but was found to be unstable. This is very likely due to the distorted cells of the curvilinear block–structured grid required by the present geometry. After completion of the transient phase average quantities, denoted by $\langle\cdot\rangle$, were accumulated over 155 and 123 time units, respectively. Below, the overbars to designate the resolved large–scale quantities are dropped.

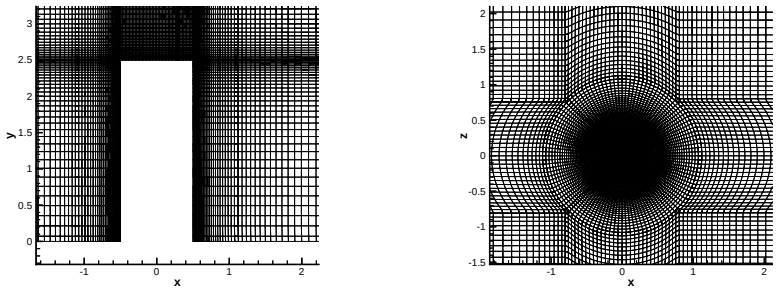

Figure 2 Zoom of the computational grid of LES1 in the vicitity of the cylinder. Left: center plane, right: plane normal to the axis above the cylinder.

5 Results

5.1 Instantaneous flow

As mentioned before, the aspect ratio H/D determines whether regular von Karman vortices are observed or not. In the visualizations of [3] no vortex shedding was observed close to the free end but two counter rotating trailing vortices with their axis almost in $x-$direction. This is in accordance with the literature, e.g. [11]. For $H/D = 2.5$ periodic antisymmetric vortices were observed at the bottom for most of the time while along the shaft intermittent symmetric and antisymmetric shedding was visualized, with vortex axes parallel to the cylinder axis. It should also be noted that for a long cylinder the spanwise correlation length in the present Reynolds number regime is $L_{z,corr} = 4D$ [12]. This gives an impression of the strength of the spanwise interaction which is to be expected also in the case of a finite length of the cylinder.

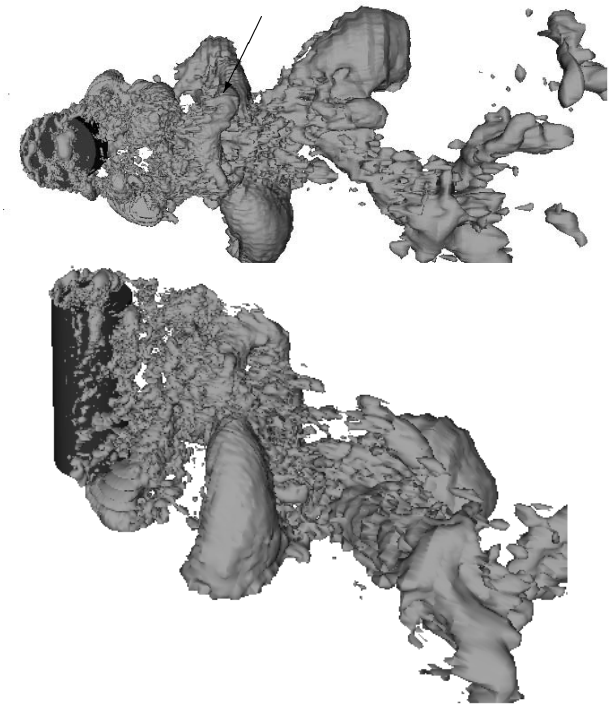

Figure 3 Three–dimensional plot of an iso–surface of the instantaneous pressure deviation, $p - \langle p \rangle = -0.05$ in LES2, viewed from the top and at an oblique angle from the rear. The arrow in the top view points to an arch–type vortex discussed in the text.

Due to the bottom–wall boundary condition the situation is somewhat different in the LES compared to the experiment. Fig.3 shows that regular von Karman

vortices are observed ranging up to about half the cylinder's height. They initially separate all along the span as claimed in [13] but are destroyed near the tip by the downward motion around the center plane. Their axis does not remain parallel to the cylinder axis but is inclined towards the center plane and smaller values of x. The latter in fact is in contrast to the sketch from [9] in Fig.1 where the inclination of the von Karman vortices is to larger x (see arrow). It seems worthwhile to investigate in future studies whether this phenomenon depends on the aspect ration H/D.

In the literature, some authors mention the appearance of two types of vortices being shed from a cylinder of finite height [14]. One is the von Karman type, the other of arch type, similar to what is observed for a wall–mounted hemisphere. The latter is reported to be observed for small H/D, the former for large aspect rations [15] and backed by pressure distributions on the ground plate. (One should however distinguish between the average flow field and pressure and the instantaneous flow which is discussed here.)

The present simulations suggest that in fact arch–type vortices are shed close to the free end even if along the shaft von Karman vortices dominate. In Fig.3 such an arch–type vortex is indicated by an arrow. It is located about half a diameter below the tip and is symmetrical with respect to the center plane ($z = 0$). Animations of pressure–perturbation surfaces show this feature even more clearly. These vortices originate on the roof of the cylinder and are sustained by the shear layer at the upper end of the recirculation zone behind the cylinder. The vortices on the roof of the cylinder are nicely visible in Fig.3. They are in turn generated by the separation at the front edge and wind around each other due to the different velocity in the recirculation bubble on the top of the roof (Fig.4 bottom left) at different heights and in and off the center plane.

5.2 Average flow

The average flow determined from LES1 and LES2 is compared to the experimental data in Fig.4 and Fig.5. For technical reasons LDA measurements can only be performed at a minimum distance from a wall. Hence, points too close to the wall were removed in Fig.5. In this way, the top left picture of this figure also gives an impression of the relatively fine grid of measurement points.

The streamlines for LES1 indicate that on the coarser grid the structure of the average flow is not correctly captured. In particular, the recirculation region is too short and there is no upward flow close to the leeward face of the cylinder. Fig.5 shows that due to the lack of resolution the recirculation also is too narrow in z–direction because the sidewall shear layer is too much inclined towards the center plane. When the finer grid is employed with LES2, the result is substantially improved as shown by the bottom pictures in Fig.4 and Fig.5. The right columns in in both figures depict the streamwise fluctuation $\langle u'u' \rangle$. In particular for LES2 these correspond fairly well to the experimental data.

Fig.6 gives more quantitative information about the computed solutions. The two sets of experimental data have been obtained with two different orientations of the LDA system. For Exp1 the beams were aligned with the y–axis, for Exp2

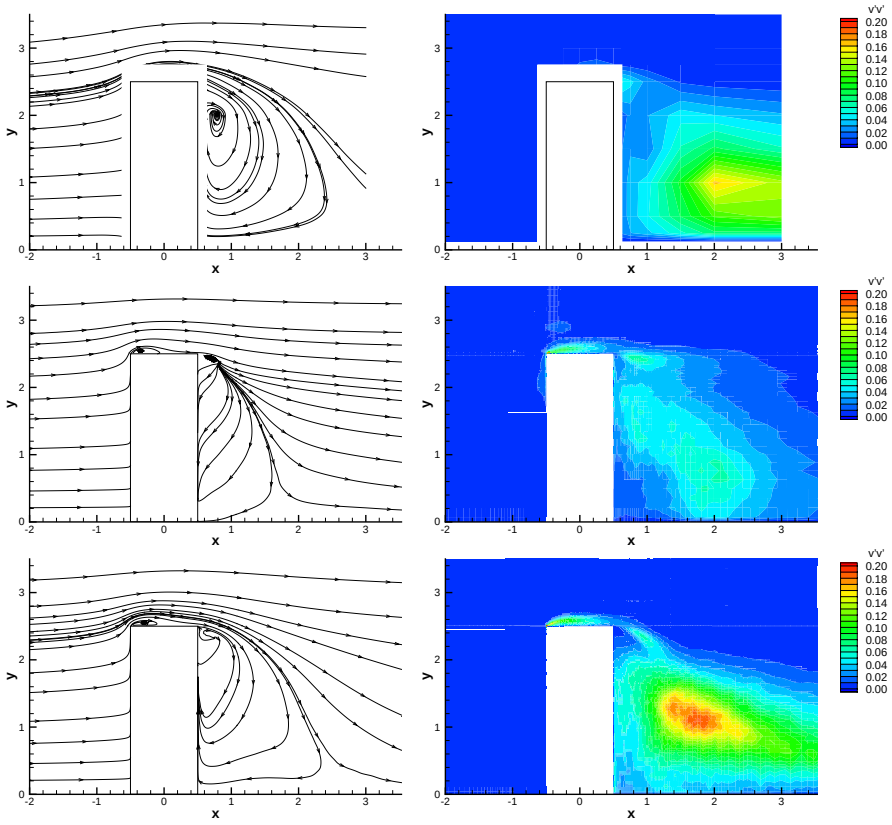

Figure 4 Cuts in center plane. Top: Experiment, middle: LES1, bottom: LES2. Left: streamlines, right: $\langle v'v' \rangle$.

aligned with the z–axis. Exp1 is therefore more precise in the shear layer, but this need not hold for the center plane. The plots show a recirculation length smaller in LES1 than in the experiment. On one hand this is due to the insufficient resolution of LES1. This is substantially improved in LES2. While still smaller when compared to Exp1 it is close to Exp2. The recovery in the wake is still somewhat faster compared to both data sets. There may however also be an impact of the different vortex shedding along the shaft discussed above which is still present for LES2. The fluctuations have substantially improved upon grid refinement and match the data of Exp2 fairly well. In the normal cuts (bottom row of Fig.6), show a very good fit of the streamwise velocity and the fluctuations along this line.

Finally, Fig.7 shows the mean pressure and the velocity vectors from LES2 in cuts at $x = const$. The tip vortex forming at the roof of the cylinder is clearly visible. Its center is located slightly below the roof at $x = 0.5$ and descends further downstream, to about $y = 1.6$ at $x = 1.0$. The maximum downward velocity in this cut is $\langle v \rangle = -0.5$.

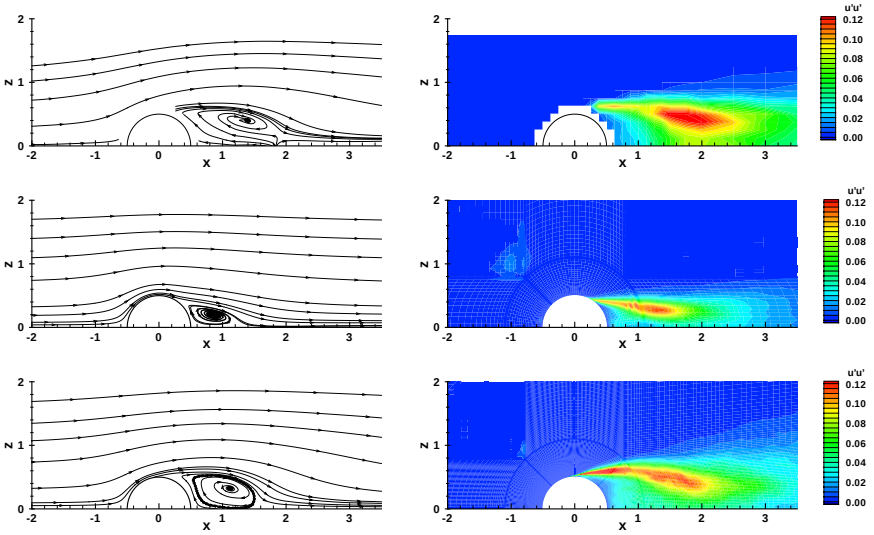

Figure 5 Cuts at $y = 1.5$. Top: Experiment, middle: LES1, bottom: LES2. Left: streamlines, right: $\langle u'u' \rangle$.

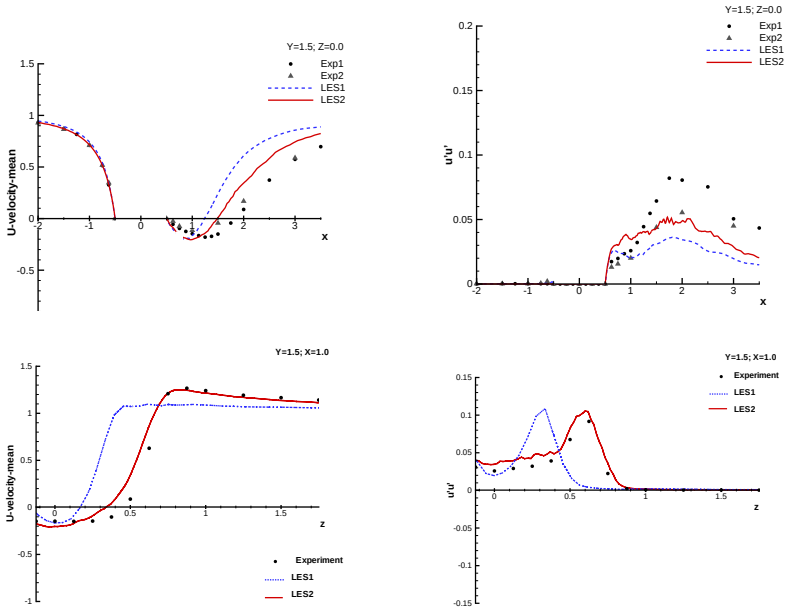

Figure 6 Average streamwise velocity (left) and corresponding fluctuations (right) along lines in the center plane and normal to the flow. Top: $y = 1.5, z = 0$, bottom: $y = 1.5, x = 1$.

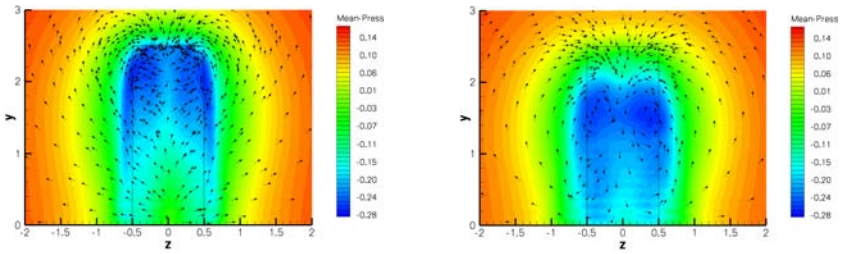

Figure 7 Cuts in planes normal to the mean flow at $x = 0.5$, i.e. immediately after the cylinder (left), and at $x = 1.0$ (right) from LES2. The gray scale replesents the average pressure, the arrows the direction of the mean flow in the plane.

6 Initial computations at EDF

Similar computations as the ones described so far were also performed with a Finite Volume code for unstructured grids recently developed at EDF. Its main features are the collocated arrangement of variables located at the center of gravity of the cells. While these can be of any shape, hexaedra have been used exclusively here. The momentum equations are solved by considering an explicit mass flux such that the three components of the velocity are uncoupled. Velocity and pressure coupling is insured by a predictor–corrector method with a SIMPLEC algorithm. The Poisson equation is solved with a conjugate gradient algorithm. For the LES calculations a second order centered scheme in space is used. Principally, a Crank-Nicholson time scheme with linearized convection is employed. Only for the part of the diffusion involving the transposed gradient operator coupling the velocity components an Adams-Bashforth extrapolation is used. This code has been successfully validated for the flow around tube bundles in [16].

The simulations were performed with the same computational domain as those with LESOCC. For cost reasons the grid employed had to be substantially coarser and contained a total of 600000 points. Fig.8 provides a zoom in the vicinity and above the cylinder. The vertical surface of the cylinder is located below the circular grid line within the area of converging grid lines. Along the cylinder shaft 26 cells were used. The physical boundary conditions were the same as used with LESOCC. To account for the coarser mesh, all solid walls were implemented with the Werner–Wengle wall law [17]. A difference is introduced by the condition on the lower wall where a solid wall was imposed. This is closer to the experimental setup but the grid is too coarse to resolve the flow in this area, even when a wall function is applied ($\Delta_z \approx 0.7\delta$).

The subgrid–scale motions were modelled with the Smagorinsky model and two computations were carried out, one with $C_s = 0.065$, the other with $C_s = 0.02$. Unfortunately, these runs could not be pursued sufficiently long to obtain fully converged statistical data. At the time of writing the first was averaged over about 4, the

second over about 12 dimensionless time units. Nevertheless, the results may serve as a guideline for further simulations of this flow.

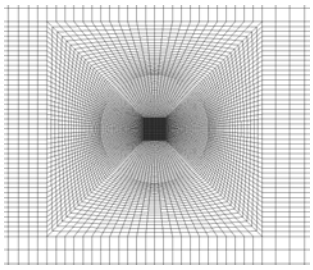

Figure 8 Zoom of the computational grid employed at EDF in the vicitity and above the cylinder.

Fig.9 shows the mean streamwise velocity in horizontal planes, similar to Fig.5. Fig.10 displays this quantity along the same lines as in Fig.6. The computation with $C_s = 0.065$ yields a result similar to LES1 above. The recirculation bubble is too small and narrow and hence the recovery of $\langle u \rangle$ in the wake is too fast. This is to some extent altered when C_s is decreased to 0.02 and the recirculation bubble becomes wider as shown in Fig.10. This observation should however be backed by pursuing the runs to obtain more reliable statistics.

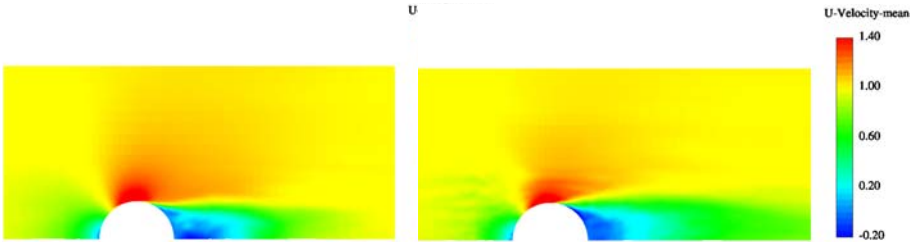

Figure 9 Average velocity at $y = 1.5$ with the unstructured code. Left: LES with $C_s = 0.065$, right: LES with $C_s = 0.02$.

7 Conclusions

The flow around a circular cylinder of finite height has been simulated with LES, assuming the bottom wall on which the cylinder is mounted to be frictionless. The

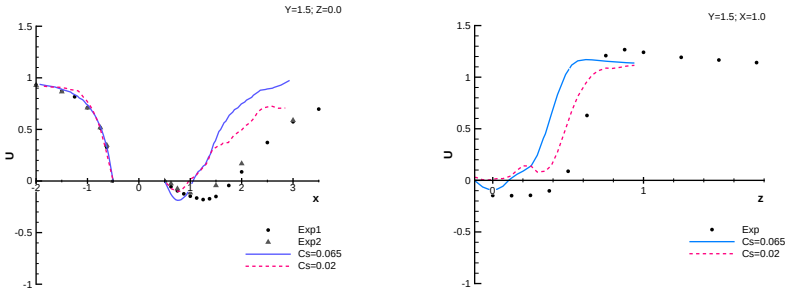

Figure 10 Average streamwise velocity along lines in the center plane and normal to the flow obtained with the unstructured code. Left: $y = 1.5, z = 0$, right: $y = 1.5, x = 1$. The curves lack smoothness due to insufficient averaging in time.

role of the bottom plate will be investigated by further computations employing a no–slip condition.

The simulations performed allow to assess the resolution demands for this configuration. Since transition occurs over the main part of the cylinder height in the separated shear layer, even when there is a thin turbulent boundary layer at the bottom wall, this area must be resolved very well. The coarser grid results show some deficiencies which are due to a lack of resolution of the transition region.

On the other hand, the flow field obtained with the finest resolution, LES2, is largely satisfactory. In particular, important information can be gained about the unsteady vortex system near the free end of the cylinder which is extremely difficult to study experimentally. Symmetric and antisymmetric shedding in form of arch vortices and von Karman vortices is observed intermittently. Here, we found that the structure of the upper part of the von Karman vortices is different from what has been proposed in the literature. This analysis will be pursued in future work.

Acknowledgments

The authors acknowledge funding through DFG and the University of Karlsruhe, the computation time was provided by the Karlsruhe Computer Center and EDF Chatou. The authors also thank M. Kappler for discussions on the experiment and for making the experimental data available and D. Laurence for useful comments.

References

[1] Fröhlich, J., Rodi, W., Kessler, P., Parpais, S., Bertoglio, J., Laurence, D.: Large eddy simulation of flow around circular cylinders on structured and unstructured grids. In Hirschel, E., ed.: Notes on Numerical Fluid Mechanics. Volume 66. Vieweg (1998) 319–338

[2] Fröhlich, J., Rodi, W., Bertoglio, J., Bieder, U., Touil, M.: Large eddy simulation of flow around circular cylinders on structured and unstructured grids, II. In Hirschel, E., ed.: Notes on Numerical Fluid Mechanics. Volume 75. Vieweg (2001) 231–249
[3] Kappler, M., Rodi, W.: Visualisation of the flow past short circular cylinders with a free end. In: Proceedings of 4th International Colloquium on Bluff Body Aerodynamics & Applications, Bochum. (2000) 613–616
[4] Kappler, M.: Experimentelle Untersuchung der Umströmung von Kreiszylinder mit ausgeprägt dreidimensionalen Effekten. PhD thesis, Institute for Hydromechanics, University of Karlsruhe (2002)
[5] Majumdar, S., Rodi, W.: Three-dimensional computation of flow past cylindrical structures and model cooling towers. Building and Environment **24** (1989) 3–22
[6] Breuer, M., Rodi, W.: Large eddy simulation of complex turbulent flows of practical interest. In Hirschel, E., ed.: Flow simulation with high performance computers II. Volume 52 of Notes on Numerical Fluid Mechanics. Vieweg, Braunschweig (1996) 258–274
[7] Mathey, F., Fröhlich, J., Rodi, W.: Large eddy simulation of the flow over a matrix of surface mounted cubes. In Biringen, S., Örs, H., Tezel, A., Ferziger, J., eds.: Industrial and Environmental Applications of Direct and Large–Eddy Simulations. Volume 529 of Lecture Nores in Physics., Springer (1999) 153–163
[8] Zdravkovich, M.: Flow Around Circular Cylinders. Oxford University Press (1997)
[9] Kawamura, T., Hiwada, M., Hibino, T., Mabuchi, I., Kamuda, M.: Flow around a finite circular cylinder on a flat plate. Bulletin of the JSME **27** (1984) 2142–2151
[10] Wieselberger, C.: Weitere Feststellungen über die Gesetze des Flüssigkeits– und Luftwiderstandes. Physik. Zeitschr. **23** (1922) 219–224
[11] Farivar, D.: Turbulent uniform flow around cylinders of finite length. AIAA journal **19** (1981) 275–281
[12] Shimizu, K., Kawamura, M.: Spanwise correlation measurement behind circular cylinder in subcritical reynolds number region. J. Phys. Soc. Jap. **32** (1972) 1454
[13] Ayoub, A., Karamcheti, K.: An experiment on the flow past a finite circular cylinder at high subcritical and supercritical reynolds numbers. J. Fluid Mech. **118** (1982) 1–26
[14] Sakamoto, H., Haniu, H., Obata, Y.: Vortex shedding from a circular cylinder placed vertically in a laminar boundary layer. Trans. Jpn. Soc. Mech. Eng. (in Japanese) **53** (1987) 714–721
[15] Taniguchi, S., Sakamoto, H., Arie, M.: Flow around a circular cylinder vertically mounted in a turbulent boundary layer. Bulletin of the JSME (1981)
[16] Banhamadouche, S., Laurence, D.: LES, coarse LES and transient RANS comparisons on the flow across a tube bundle. In Fueyo, N., Rodi, W., eds.: Engineering Turbulence Modelling and Experiments 5. (to appear 2002)
[17] Werner, H., Wengle, H.: Large–Eddy Simulation of turbulent flow over and around a cube in a plane channel. In Durst, F., Friedrich, R., Launder, B., Schmidt, F., Schumann, U., Whitelaw, J., eds.: Selected Papers from the 8th Symposium on Turbulent Shear Flows, Springer (1993) 155–168